Progress in Neuropsychopharmacology & Biological Psychiatry 137 (2025) 111270

Contents lists available at ScienceDirect

Progress in Neuropsychopharmacology & Biological Psychiatry

journal homepage: www.elsevier.com/locate/pnp

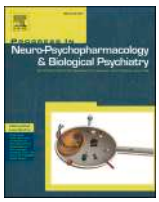

# Local cortical structure pattern and genetic links in schizophrenia: An MRI and CRISPR/Cas9 study

Pei-Shan Hou [a,b,c,**], Shu-Fei Lin [a], Jun-Ding Zhu [d,e], Chih-Yun Chung [a], Shih-Jen Tsai [b,f], Albert C. Yang [b,c,g,h,i,*]

[a] Institute of Anatomy and Cell Biology, National Yang Ming Chiao Tung University, Taipei 11221, Taiwan
[b] Institute of Brain Science, National Yang-Ming Chiao Tung University, Taipei 11221, Taiwan
[c] Brain Research Center, National Yang-Ming Chiao Tung University, Taipei 11221, Taiwan
[d] Department of Occupational Therapy, College of Medical Science and Technology, Chung Shan Medical University, Taichung 40201, Taiwan
[e] Occupational Therapy Room, Chung Shan Medical University Hospital, Taichung 40201, Taiwan
[f] Department of Psychiatry, Taipei Veterans General Hospital, Taipei, Taiwan
[g] Digital Medicine and Smart Healthcare Research Center, National Yang Ming Chiao Tung University, Taipei, Taiwan
[h] Department of Medical Research, Taipei Veterans General Hospital, Taipei, Taiwan
[i] School of Medicine, National Yang Ming Chiao Tung University, Taipei, Taiwan

ARTICLE INFO

*Keywords:*
schizophrenia
Brodmann area
structural pattern index
genetic analysis
neocortex
CRISPR/Cas9

ABSTRACT

While the etiology of schizophrenia (SZ) remains elusive, its diverse phenotypes suggest the involvement of distinct functional cortical areas, and the heritability of SZ implies the underlying genetic factors. This study aimed to integrate imaging and molecular analyses to elucidate the genetic underpinnings of SZ. We investigated the local cortical structural pattern changes in Brodmann areas (BAs) by calculating the cortical structural pattern index (SPI) using magnetic resonance imaging analysis from 194 individuals with SZ and 330 controls. Significant local structural changes were detected in certain Brodmann areas in symmetric or asymmetric patterns, such as symmetric changes in the BA4 primary motor area and BA23 part of posterior cingulate cortex, and asymmetric changes in the BA13 insula, BA11 inferior orbitofrontal area, and BA 24, and BA 31 cingulate cortex. Following genome-wide association tests, we found genetic variants and SNP-mapped genes and verified the areal preferential expression profiles in the developing human and mouse neocortex. Finally, we performed a loss-of-function analysis using the CRISPR/Cas9 system to investigate the effects of disrupting the SZ-related SNP-mapped Morf4l1, Reep3, or Tmed3 gene on cortical cell fate to understand their roles in generating appropriate composition of cortical neurons. This study outlines a pipeline for identifying local structural changes, associated genetic causes, and potential molecular mechanisms underlying mental disorders. Additionally, these data shed light on establishing a structurally integral cerebral cortex for higher cognitive functions.

## 1. Introduction

Schizophrenia (SZ), a severe and diverse psychiatric disorder, exhibits symptoms such as hallucinations, delusions, negative symptoms, and cognitive impairments. Previous studies revealed variable phenotypes with different mechanisms implicated, including dopamine pathway associations and abnormal morphology at distinct anatomical structures (Banaj et al., 2023; Lewis and González-Burgos, 2008). Alongside these complexities, SZ is highly heritable, as evidenced by family and twin research (Kety, 1987; Sullivan et al., 2003). Anatomical abnormalities in SZ, such as grey matter volume loss in the insula and anterior cingulate cortex and cortical thinning in the temporal and prefrontal cortex, highlight region-specific alterations and underscore regulatory complexity in various brain regions (Bora et al., 2011; Sugihara et al., 2017). Despite recognizing symptoms, the pathological causes and genetic factors underlying SZ remain unclear.

* Corresponding author at: School of Medicine/Digital Medicine and Smart Healthcare Research Center, National Yang Ming Chiao Tung University, Taipei, Taiwan.
** Corresponding author at: Institute of Anatomy and Cell Biology, National Yang Ming Chiao Tung University, Taipei, Taiwan.
*E-mail addresses:* pshou@nycu.edu.tw (P.-S. Hou), accyang@nycu.edu.tw (A.C. Yang).

https://doi.org/10.1016/j.pnpbp.2025.111270
Received 19 September 2024; Received in revised form 5 January 2025; Accepted 21 January 2025
Available online 23 January 2025

Daily tasks, like processing sensory stimuli and cognitive thinking, rely on distinct cerebral cortex functional areas. Korbinian Brodmann identified 52 cortical areas via the arrangement of cortical cells as Brodmann areas (BAs) (Brodmann, 1909). Unique cell components in an area define its functions. For instance, Brodmann area 13 (BA13) and 16 (BA16) compose the insula, integrating sensory and emotional functions, behavioral motivation, learning, and memory by connecting to multiple cortical regions. Trajectories exist between the insula cortex (BA13 and BA16), anterior cingulate cortex, medial prefrontal cortex, and orbitofrontal cortex, contributing to cognitive and emotional functions like fear (Etkin et al., 2011). The insula (BA13 and BA16) is a hotspot for psychiatric disorders like SZ, with observed reductions in grey matter volume and cortical thickness (Schlaepfer et al., 1994; Sheffield et al., 2020; Shepherd et al., 2012). BA38, in the temporal pole, is associated with visual cognition, language processing, and socio-emotional functions (Herlin et al., 2021). Recent studies showed reduced cortical thickness in the temporal pole (BA38) in individuals with neurodegenerative disorders (LaPoint et al., 2017) and SZ (van Erp et al., 2018).

The human cerebral cortex comprises grey matter, organized into a six-layered structure of cortical neurons, and white matter, housing neuronal projections. Cortical neurons, especially excitatory projection neurons in each layer, perform distinct functions. For instance, deep-layer Ctip2 or Tbr1-expressing neurons project to extra-cortical areas (e.g., spinal cord or thalamus) for interaction with the external environment, while upper-layer Satb2 or Brn2-expressing neurons project to other cortical areas, integrating signals for higher cognitive function (Ozkan et al., 2020). Interestingly, individuals with SZ exhibit decreased thickness in the upper layer, suggesting a potential cause for impaired higher cognitive function (Wagstyl et al., 2016). Beyond diverse functions, the functions in BAs are primarily defined by the cell composition of excitatory projection neurons. For example, the primary motor area (BA4) contains more deep-layer neurons than the adjacent primary somatosensory area (BA1, 2, and 3), with a sharp cytoarchitectural boundary easily recognized (Brodmann, 1909). Given the conserved arrangement of cytoarchitecture among individuals, the establishment of BAs and their distinguishable boundaries during neurodevelopment should be regulated by intrinsic factors. Impairment in the developmental process may lead to abnormalities in cortical connectivity, as observed in individuals with SZ.

Diagnosing and treating psychiatric disorders, such as SZ, remains challenging due to diverse symptoms. A potential solution involves decoding connections between traits and related molecular mechanisms. In this study, we combined the neuroimaging and genetic analyses to assess the linkage between the phenotypes and the genotypes. Research on the genetic influences on brain structure reveals complex heritability patterns across various regions. Voxel-based morphometry (VBM) studies have demonstrated high heritability for global brain volumes and cortical thickness, with significant regional variability (Eyler et al., 2012; Rimol et al., 2010). Traditional VBM analyses primarily focus on gross volumetric changes; however, this method may overlook subtle and spatially complex differences (Davatzikos, 2004). In this study, the structural pattern index (SPI) was calculated by determining the standard deviation of grey matter volume and cortical thickness for each voxel (i.e., grey matter volume) or vertex (i.e., cortical thickness), along with their neighboring voxels or vertices. This approach enabled a nonlinear assessment of local cortical structural patterns. Therefore, this study aimed to investigate genetic causes of local cortical structural pattern changes in BAs by calculating the cortical SPI using magnetic resonance imaging (MRI) data and performing GWAS analysis from SZ and control groups.

## 2. Materials and methods

### 2.1. Participants

MRI and DNA phenotypic data of 524 individuals in this study, including 194 individuals with SZ and 330 healthy controls (HCs), were obtained from the Taiwan Aging and Mental Illness (TAMI) database (Zhu et al., 2023a, 2023b). Our analysis of demographic data indicated that the two groups were comparable in age ($p = 0.85$). Individual with SZ had an average age of 43.25 years (SD = 11.93, range = 20–70 years), while HCs had an average age of 43.49 years (SD = 15.47, range = 20–84 years). Furthermore, the gender distribution was consistent across both groups, with no statistically significant differences observed ($p = 0.28$). However, significant differences were observed in educational year and cognitive functioning, as assessed by the Mini-Mental State Examination (MMSE). HCs had a significantly higher average education year than individuals with SZ ($p < 0.001$). Similarly, MMSE scores were significantly greater in the healthy control group ($p < 0.001$). In addition, individuals with SZ reported an average illness duration of 15.56 years (SD = 10.30, range = 0–38 years). A comprehensive summary of the demographic characteristics and cognitive assessments is provided in Table 1.

### 2.2. MR image acquisition and preprocessing

All T1-weighted MRI data acquired by 3 T MRI scanner (Siemens Magnetom Tim Trio, Erlangen, Germany) with sagittal 3D magnetization-prepared rapid gradient echo (MPRAGE) model at National Yang Ming Chiao Tung University. The scanning protocol and parameter setting were described previously (Zhu et al., 2023a, 2023b). Briefly, the sequence parameters were as follows: repetition time (TR) of 2530 ms, echo time (TE) of 3.5 ms, inversion time of 1100 ms, matrix size of 256 × 256, 192 slices with a thickness of 1 mm, voxel size of 1.0 × 1.0 × 1.0 mm3, and a flip angle of 7°. The study received approval

**Table 1**
Summary of the demographic characteristics and clincial assessments of SZ and HC participants.[a, b, c]

| Characteristics | SZ ($n = 194$) | HC ($n = 330$) | Statistic (t or $\chi^2$) | $p$ value |
|---|---|---|---|---|
| Sex<br>Male, n (%)<br>Female, n (%) | <br>85 (43.8 %)<br>109 (56.2 %) | 129 (39.1 %)<br>210 (60.9 %) | 1.13 | 0.28 [b] |
| Age, year (SD) | 43.25 (11.93) | 43.49 (15.47) | 0.20 | 0.85 [a] |
| Education level, year (SD) | 12.50 (3.55) | 15.85 (3.85) | 9.90 | < 0.001 [a] |
| MMSE (SD) | 26.81 (3.39) | 28.96 (1.01) | 8.59 | < 0.001 [a] |
| Illness duration, year (SD) | 15.56 (10.30) | – | – | – |
| PANSS score (SD) | | | | |
| Total | 42.04 (10.76) | – | – | – |
| Positive symptoms | 10.74 (3.37) | – | – | – |
| Negative symptoms | 10.04 (3.76) | – | – | – |
| General psychopathology symptoms | 21.26 (5.18) | – | – | – |
| CPZ equivalent dosage [c] (SD) | 402.42 (324.27) | – | – | – |

Data are mean (SD) or n (%) unless specified otherwise. Abbreviations: SZ, individuals with schizophrenia; HC, healthy control; MMSE, Mini-Mental State Examination; PANSS, Positive and Negative Syndrome Scale; CPZ, chlorpromazine.

[a] Independent $t$-test, significance level = 0.05.

[b] Chi-square test, significance level = 0.05.

[c] Only 161 individuals with schizophrenia had verified medication records.

from the Institutional Review Board of both Taipei Veterans General Hospital and National Yang Ming Chiao Tung University. All participants provided written informed consent.

The T1-weighted MRI data underwent preprocessing using the Statistical Parametric Mapping (SPM) 12, the Data Processing & Analysis for Brain Imaging (DPABI) toolbox (Yan et al., 2016) and FreeSurfer software. For volume-wise SPI analysis, the workflow of raw T1-weighted MRI preprocessing followed the steps (Fig. 1A): (1) all images were manually oriented using the anterior commissure-posterior commissure line as a reference, (2) the brain tissue was extracted through the removal of the skull, (3) all images were normalized to conform to the MNI standard space with a voxel size of 1 mm × 1 mm × 1 mm for further analysis. (4) the images were subsequently segmented into specific tissue types: grey matter, white matter, and cerebrospinal fluid (CSF). After segmentation, grey matter volume was obtained by concentration, which was given by the probability of the target tissue type in a certain region. For thickness-wise SPI analysis, reconstruction of a 2D inflated cortical surface from a three-dimensional volume was processed using a "recon-all" algorithm in Freesurfer software with version 6.0.0 (https://surfer.nmr.mgh.harvard.edu/). To obtain cortical thickness, boundaries of different tissue types formed into surfaces by building mesh with faces and vertices in reconstruction, which allowed surface transformation. Calculation of cortical thickness in each vertex is defined by the shortest distances between boundaries of grey/white matter (white surface) and CSF/grey matter (pial surface). Registrations were performed by Freesurfer built-in function "mris_surf2surf" to a surface-based standard template "fsaverage".

### 2.3. Atlas modification

The Brodmann's map template for volume-wise SPI analysis was obtained from the MRIcron software (https://www.nitrc.org/projects/mricron), and the Brodmann's map template for thickness-wise SPI analysis was obtained from the Freesurfer software created by Van Essen lab (https://sites.wustl.edu/vanessenlab/resources/). To label the undefined areas of interest in these two original templates, volume-wise SPI analysis, areas 13 (insula) and 31 (dorsal posterior cingulate cortex) were modified. We extracted the insula (33,34) from the automated anatomical labeling (AAL) (Rolls et al., 2020) as area 13. For area 31, first, we obtained the middle cingulate cortex (37.38) from AAL Field (Rolls et al., 2020), which includes dorsal and ventral cingulate cortex on the posterior side, so we refilled the ventral cingulate cortex, which is the area 23 and 24, to identify the dorsal part. For thickness-wise SPI analysis, area 13 (insula) was modified, and regions in the insula from Destrieux Atlas (Destrieux et al., 2010) were utilized (Fig. S1).

### 2.4. Structural pattern index, SPI

To calculate the thickness-wise and volume-wise SPIs, neighboring vertices and voxels were selected to characterize local cortical structure patterns. For cortical thickness analysis, 5–6 neighboring vertices were included for each vertex, whereas 26 neighboring voxels were considered for each voxel in the grey matter volume analysis.

For the thickness-wise SPI analysis, neighboring vertices were identified using the FreeSurfer built-in function "mris_convert." FreeSurfer employs a spherical-based cortical registration method, where each vertex on the reconstructed cortical surface is typically connected to six neighboring vertices. However, in certain boundary regions—such as trimmed meshes or incompletely closed surfaces—this connectivity may be reduced, resulting in some vertices being connected to fewer than six neighbors (Dale et al., 1999; Fischl, 2012; Fischl et al., 1999). Therefore, the thickness-wise SPI was calculated by measuring the standard deviation of cortical thickness across each vertex and its neighboring vertices (i.e., 5–6 vertices). This standard deviation was defined as the SPI value for the corresponding core vertex. This process was applied to the entire brain, obtaining a whole-brain thickness-wise SPI map for each participant. Similarly, for the volume-wise SPI, we computed it by measuring the standard deviation of grey matter volume

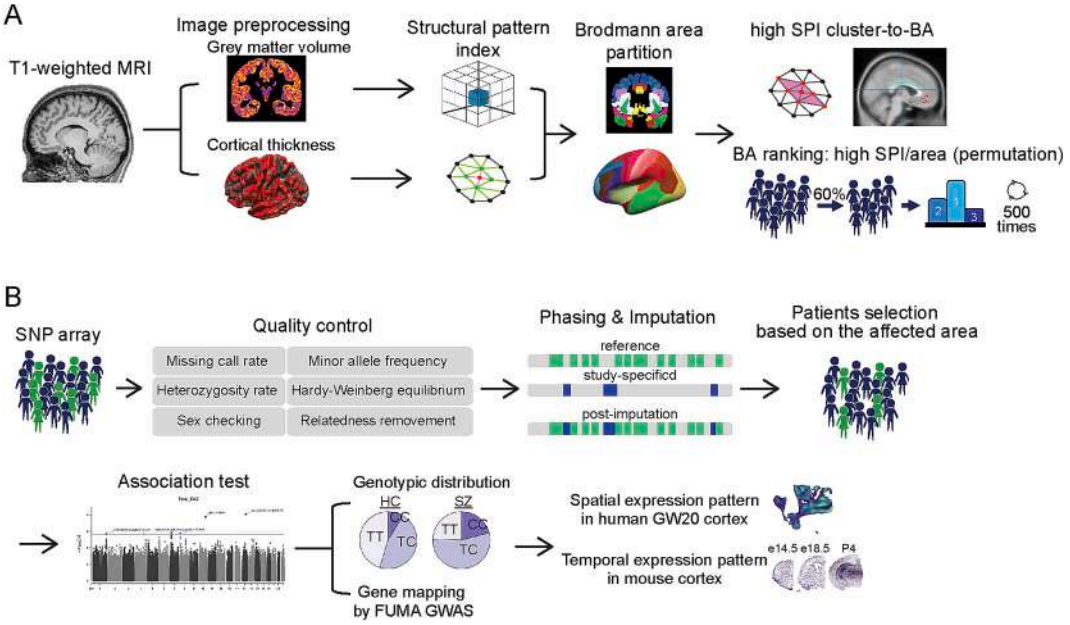


**Fig. 1. The workflow of identifying affected Brodmann areas and correlated genes.**
(**A**) Workflow for T1-weighted MRI analysis to identify Brodmann areas that are affected by schizophrenia: imaging preprocessing, calculating structural pattern index, partitioning Brodmann areas, and annotating Brodmann areas with high SPI clusters or ranking BA using high SPI per area with permutation. (**B**) Workflow for genome-wide association testing to identify genes potentially affected by schizophrenia. The procedure includes SNP array analysis, quality control, phasing and imputation to fill the missing SNPs, selecting patients whose SPI in certain BA were significantly compared to healthy control, conducting association test, Analyzing genotypic distribution and mapping associated genes using FUMAGWAS (https://fuma.ctglab.nl), evaluating genes based on scRNA sequencing analysis using human GW20 neocortex(Bhaduri et al., 2021) and dynamic mRNA expression profiles in developing mouse brains. BA, Brodmann area; SPI, structural pattern index; SNP, single nucleotide polymorphism; GW, gestational weeks.

across each voxel and its respective neighboring voxels (i.e., 26 voxels). This standard deviation was defined as the SPI value for the corresponding core voxel. This process was applied to the entire brain, obtaining a whole-brain volume-wise SPI map for each participant.

### 2.5. SNP genotype distribution and gene mapping

Individual genotypes were examined using Axiom Genome-Wide TWB 1.0 Array Plate (Affymetrix) with 653,291 tagged SNPs based on the GRch37/hg19 chromosome. Quality control was performed using PLINK (version 1.9) (Purcell et al., 2007) and PLINK2 (version 2.0) (Chang et al., 2015) (Fig. 1B). A total of 404 samples, with 232 controls and 172 cases (183 males and 221 females), and 590,776 SNPs were obtained. Haplotype phasing and genotype imputation were performed to improve the statistical power using Eagle (version 2.4.1, https://alkesgroup.broadinstitute.org/Eagle) (Loh et al., 2016a, 2016b; Loh et al., 2016a, 2016b) on the Michigan Imputation Server (version 1.0.2, https://imputationserver.sph.umich.edu) (Das et al., 2016) and Impute5 (Rubinacci et al., 2020), respectively, with the 1000 Genomes Project phase 3v5 East Asian population panel as references (Genomes Project, C., et al., 2015). A total 5,813,972 SNPs were obtained. R language was used to summarize the genotype distribution for HC and SZ participants. A pie chart, created using the R package "ggplot2," visualized this distribution. The gene mapping process for affected SNPs was conducted through the FUMA GWAS server (https://fuma.ctglab.nl), utilizing the SNP2GENE function, which includes positional and eQTL mapping. ANNOVAR annotated functional regions of genes using significant SNPs (leading SNPs) and surrounding genomic loci in linkage disequilibrium (LD) structure(Wang et al., 2010). For positional mapping, genes within 10 kb of leading SNPs were identified. EQTL mapping employed mRNA expression data from various tissue types, utilizing databases such as GTEx (Aguet et al., 2020), Blood eQTL browser (Westra et al., 2013; Zhernakova et al., 2017), and BRAINEAC (Ramasamy et al., 2014).

### 2.6. Animals and sample collection

ICR mice used in this study were hosted in the Laboratory Animal Center of the National Yang Ming Chiao Tung University Laboratory Animal Center. All experiments were performed following the instructional guidelines approved by the Institutional Animal Care and Use Committee (IACUC) No. 1081010 and guidelines published in the Institute of Laboratory Animals Resources Commission on Life Sciences 1996 (Care, and O. L. A. R. C. O., and Animals, U. O. L, 1986). The embryonic day was defined by the time of vaginal plug detection at noon of the day (E0.5) after mating the night before. Collection of mouse brains from E14.5, E18.5, P4, and P7, the preparation of cryosections for ISH and floating sections for immunostaining analysis, and immunostaining analysis were performed following the procedure published previously (Hou et al., 2019). For E18.5, P4, and P7, embryos and pups were perfused with PBS, followed by 4 % paraformaldehyde (PFA) before brain collection. For E14.5, embryonic brains were collected directly without the perfusion step. For in situ hybridization, the brain samples were stored in 4 % PFA at 4 °*C. prior* to cryosectioning, the samples were immersed in 30 % sucrose-PBS at 4 °C overnight and subsequently embedded with cryomatrix (Thermo) compound. Serial coronal sections were obtained using a cryostat machine (Thermo CryoStat NX70). Sections with a thickness of 12 μm were prepared for E14.5 and E18.5 brains, and sections with a thickness of 14 μm were prepared for P4 brains. All sections were stored at −80 °C. For in-utero electroporation, the brain samples at P7 were stored in 2 % PFA 4 °C overnight and transferred to PBS at 4 °C. The samples were embedded with 1.4 % agarose and 1 % gelatin in PBS before coronal sectioning by a vibratome slicer with 100 μm thickness. The floating sections were stored in 0.1 % sodium azide in PBS at 4 °C.

### 2.7. Immunostaining analysis

Immunostaining analyses were performed following the procedure published previously (Hou et al., 2019). Briefly, after washing the brain slices with PBST (0.2 % Tween 20 in PBS), the blocking step was performed at room temperature for 4 h using 10 % normal donkey serum, 0.3 % Triton X-100, and 0.1 % sodium azide in PBS. The primary antibodies were applied 3 overnight at 4 °C in 1 % normal donkey serum, 0.3 % Triton X-100, and 0.1 % sodium azide in PBS, as follows: rat anti-CTIP2 antibody (1:2000, abcam); chicken anti-GFP antibody (1:10000, abcam); mouse anti-Rorβ antibody (1:500, abcam); rabbit anti-Brn2 antibody (1:2500, abcam); rat anti-GFP antibody (1:10000, abcam); rabbit anti-Tbr1 antibody (1:2000, abcam). Following PBST washing, the slices were incubated at 4 °C overnight with the following Alexa Fluor-conjugated secondary antibodies: donkey anti-chicken 488, donkey anti-rat 488, donkey anti-rat 594, donkey anti-mouse 594, and donkey anti-rabbit 647 (1:1000, Invitrogen), in 1 % normal donkey serum, 0.3 % Triton X-100, and 0.1 % sodium azide in PBS. Nuclei were stained with DAPI. The slides were mounted using an antifade mounting medium (Vector). Images were acquired using an LSM700 confocal microscope (Carl Zeiss). The *p*-value was calculated using a built-in function in Excel software.

### 2.8. Preparation of probes and in situ hybridization, ISH

Probe preparation followed previously published procedures (Hou et al., 2017). The DNA template for ISH probes were amplified by PCR using the probes listed in Supplementary Table 7 followed by T7 promoter tagging PCR using forward, ATTAGGTGACACTATAGAAGGCCGCGG; reverse, TAATACGACTCACTATAGGGCCCGGGGC. Purified promoter-tagged PCR products were subjected to in vitro transcription using T7 RNA polymerase and Digoxigenin (DIG) Labeling Mix (Roche). In situ hybridization (ISH) was performed following the procedure previously described (Hou et al., 2017). First, cold 4 % PFA was used to perform post-fixation for 10 mins, and then 1.5 % $H_2O_2$-MeOH for 15 mins, 0.2 N HCl-H2O for 8 mins, and 10 μg/ml proteinase K (BioShop) for 5 mins. Slides were post-fixed again by 4 % PFA on ice and then followed by an acetylation step for 10 mins. DEPC-PBS was used to wash slides between the above steps for 5 mins. 300 ng/ml probes in hybridization buffer were heated at 80 °C before slides, and then the hybridization reaction was performed in a 55 °C oven overnight. Slides were treated with 5× SSC for 10 mins at 65 °C and 50 % formamide/2× SSC at 65 °C for 30 mins before RNaseA treatment at 37 °C for 30 mins. After washing with RNase buffer at 37 °C for 15 mins, 50 % formamide/2× SSC at 65 °C twice, and 2× and 0.1× SSC at 37 °C for 15 mins, blocking steps were performed using 1 % Blocking Reagent (BB1) (Roche) at 37 °C for 30 mins. Anti-DIG-POD antibody (Roche) in BB1 was applied and incubated at 4 °C overnight. After rinsing with a washing buffer, the slides were blocked by BB2, which contained 0.5 % casein, 150 mM sodium chloride, and 100 mM Tris-HCl pH 7.5. Biotinyltyramide in diluent buffer was then applied for 15 mins at 37 °C followed by streptavidin-AP (Roche) in 1 % BB1 at room temperature for 1 h. Signals were developed using the NBT/BCIP method, and the slides were mounted using a CC mount (Sigma). Images were acquired using the Zeiss Axioscan 7 microscope slide scanner.

### 2.9. CRISPER/Cas9 constructs and in-utero electroporation

A pair of single guide RNA (sgRNA) to target the start codon of *Morf4l1* gene was designed (http://chopchop.cbu.uib.no): Morf4l1_5', TGTGCGTAGCGGTTAGCCGTTGG; Morf4l1_3', AAGCGGCACACTCACCCTCCTGG. The plasmid was constructed following the procedure published previously (Sakuma et al., 2014). To anneal oligonucleotides, an annealing buffer containing 100 mM Tris–HCl pH 8 and 50 mM NaCl, and a delta thermal cycle, 95 °C for 10 min, then decreased 5 degrees per minute until 25 °C, were used. The annealed

oligonucleotides were used to construct CRISPR/Cas9 plasmids. The plasmid was delivered into the developing neocortex at E13.5 following the procedure published previously (Hou et al., 2019). Briefly, before the surgery, E13.5 pregnant mice were anesthetized with pentobarbital via intraperitoneal injection. The uterus was exposed with midline laparotomy. DNA solution, which contains 1 μg/μl pCAG-GFP and 1 μg/μl KO constructs or 1 μg/μl pCAG-GFP and 1 μg/μl Cas9 only constructs, in 0.05 % fast green in Hanks' balanced salt solution (HBSS) was microinjected into the lateral ventricles using capillaries. Electroporation was performed using platinum electrodes, and the condition was 33 V with a 50-ms on/950-ms off period for 4 cycles.

### 2.10. Statistical analysis

As the behavior results from interconnected computations between different functional cerebral areas, we next asked whether these regions with changed SPI in SZ group compared to the HC group were restricted to certain BAs. To address this, we applied two approaches to explore the corresponding functional regions on Brodmann's map: structural morphology analysis and ratio analysis. The mean SPI for each voxel/vertex in HC and SZ groups was calculated by MATLAB R2022a. A generalized linear model (GLM) was performed using the Statistics and Machine Learning Toolbox of MATLAB; t-map and p-map are t statistics and *p*-value for coefficient estimates, respectively. For volume-wise SPI analysis, significant brain clusters were recorded if the p-value corrected by the family-wise error rate (FWE) was less than 0.05 at the cluster level, with a minimum of 100 voxels in the cluster. The t-map was visualized using xjView toolbox (http://www.alivelearn.net/xjview) and BrainNet Viewer (https://www.nitrc.org/projects/bnv/) (Xia et al., 2013). In thickness-wise SPI analysis, cluster correction was performed by Freesurfer-built-in function "mri_glmfit-sim". The p-value, corrected for FWE, was defined as less than 0.05 at the cluster level. Visualization was displayed with the Freesurfer-built-in application "Freeview.app".

In permutation simulation with 5000 repetitions, we randomly extracted 60 % of samples from the dataset applied with GLM by MATLAB. Regional ranking was processed by calculating the ratio of significant voxels/vertices in each area and ranking all areas. The affected areas were selected by ranking, the mean value of which was not greater than 10. Given that the number of voxels exceeds the number of vertices, and to minimize the risk of Type I errors associated with multiple comparisons, we implemented stricter p-value thresholds to define statistical significance for the thickness-wise and volume-wise SPI analyses. Specifically, p-value thresholds of less than 1e-4 and 1e-5 were applied for the thickness-wise and volume-wise SPI analyses, respectively. A 2D-density plot was generated by the R package "ggplot2" (Wickham, 2016).

In addition, we conducted correlation analyses between PANSS scores (including the positive subscale, negative subscale, general psychopathology subscale, and total score) and SPI maps (thickness-wise SPI and volume-wise SPI) in schizophrenia to investigate the relationship between SPIs and symptom severity.

## 3. Results

### 3.1. Distinct functional areas affected by SZ in structural morphology analysis

In thickness-wise SPI analysis, a total of 10 significant clusters were observed, including 3 clusters (tL2, tL5, tL6) in the left primary motor area (BA4) and 1 cluster (tR3) in the right primary motor area (BA4), 1 cluster (tL4) in the left insula (BA11), 2 clusters (tL1, tL3) in the left temporal pole (BA38), 1 cluster (tL7) in the left primary auditory cortex and 2 clusters (tR1, tR2) in the right inferior orbitofrontal area (BA11) (Fig. 2A, Supplementary Fig. 2A and 2B, Supplementary Table 1). In addition, we found that the SZ group had higher thickness-wise SPI in 4 clusters (i.e., tL2, tL5, tL6, and tR3), while lower thickness-wise SPI was found in 6 clusters compared to the HC group (i.e., tL1, tL3, tL4, tL7, tR1 and tR2).

In volume-wise SPI analysis, we found that the SZ group had significantly greater volume-wise SPI than the HC group in 3 clusters, including the left inferior orbitofrontal area (BA11), the left insula (BA13), and the left posterior caudal fusiform gyrus and left inferior temporal area (BA37). In addition, 5 clusters in the SZ group showed lower volumetric SPI compared to the HC group, such as the left temporal pole (BA38), the left anterior ventral cingulate cortex (BA24), the left inferior primary auditory cortex (BA42), the right pars orbitalis (BA47) and the right posterior dorsal cingulate cortex (BA31) (Fig. 2B, Supplementary Fig. 2C and 2D, Supplementary Table 2). Taken together, we found that the clusters in volume-wise analysis occupied bigger areas than in thickness-wise analysis, and the left BA38 temporal pole had the highest ratio of changed SPI in both thickness-wise and volume-wise analysis.

Next, we performed a ratio analysis. We calculated and ranked the ratio of changed SPI ($p$-value $<0.00001$) in the BA. In addition, to ensure the results faithfully represent the effects of SZ in the population, we applied a permutation test by randomly sampling 60 % of our datasets and repeating the ratio analysis 5000 times. The results were shown in density plots (Fig. 3A and B) and summarized in Supplementary Table 3. We found that the results of the ratio analysis were similar to the structural morphology analysis in terms of asymmetric effects and the BAs (Fig. 2A and 3A, and Supplementary Table 1 and 3). In most permutation tests, BA4 was high-ranked in both the left and right hemispheres, BA11 was high-ranked in the right hemisphere, and BA13 and BA38 were high-ranked in the left hemisphere.

In volume-wise SPI analysis, variable results in the ratio analysis were found as compared to those in the structural morphology analysis. Similar to the results of the structural morphology analysis, BA31 was high-ranked in the right hemisphere, and BA11, BA13, BA24, and BA38 were high-ranked in the left hemisphere (Fig. 2B, C and 3B, and Supplementary Table 2 and 3). Interestingly, different from the results of the structural morphology analysis, BA23 was high-ranked in both the left and right hemispheres, and BA13, BA25, BA34, and BA38 were high-ranked in the right hemisphere. In contrast, no high-ranked results were detected in left BA37 and left BA42 (Fig. 2B, C and 3B, and Supplementary Table 2 and 3). Taken together, the variable results between structural morphology and ratio analyses may demonstrate the diverse extent of disease-associated local morphological alterations among BAs in individuals with SZ (Fig. 2, 3A, and B).

For the correlation analysis, we found that BA 29 (i.e., the posterior cingulate cortex) exhibited a significant positive correlation with the PANSS total score (FWE-corrected $p = 0.0002$) in the thickness-wise SPI map. However, no other significant associations were observed between symptom severity and other regions in either the thickness-wise or volume-wise SPI maps in schizophrenia.

### 3.2. Correlation between specific SNPs and BAs

Next, we aimed to decipher the underlying genetic factors that may contribute to the local structural changes in certain BAs in individuals with SZ. To this, we obtained DNA phenotypic data from the TAMI database and performed preprocessing procedures, including quality control, phasing, and imputation (Fig. 1B). Quality control by PLINK ensured the reliability of our results in genome-wide association studies (GWAS) analysis. After quality control, DNA phenotypic data from 404 participants (232 HCs and 172 individuals with SZ) and 5,813,972 variants were used for subsequent analyses (see Materials and Methods for detailed procedures).

To identify disease-associated genetic variants in individuals with SZ, we performed GWAS, and between HC and SZ groups, SNPs on chromosomes 10 (rs670625) and 15 (rs12232282) were detected with the suggestive associations ($p < 1e\text{-}6$) (Supplementary Fig. 3A). Next, to investigate whether certain SNPs are correlated with the changes in the

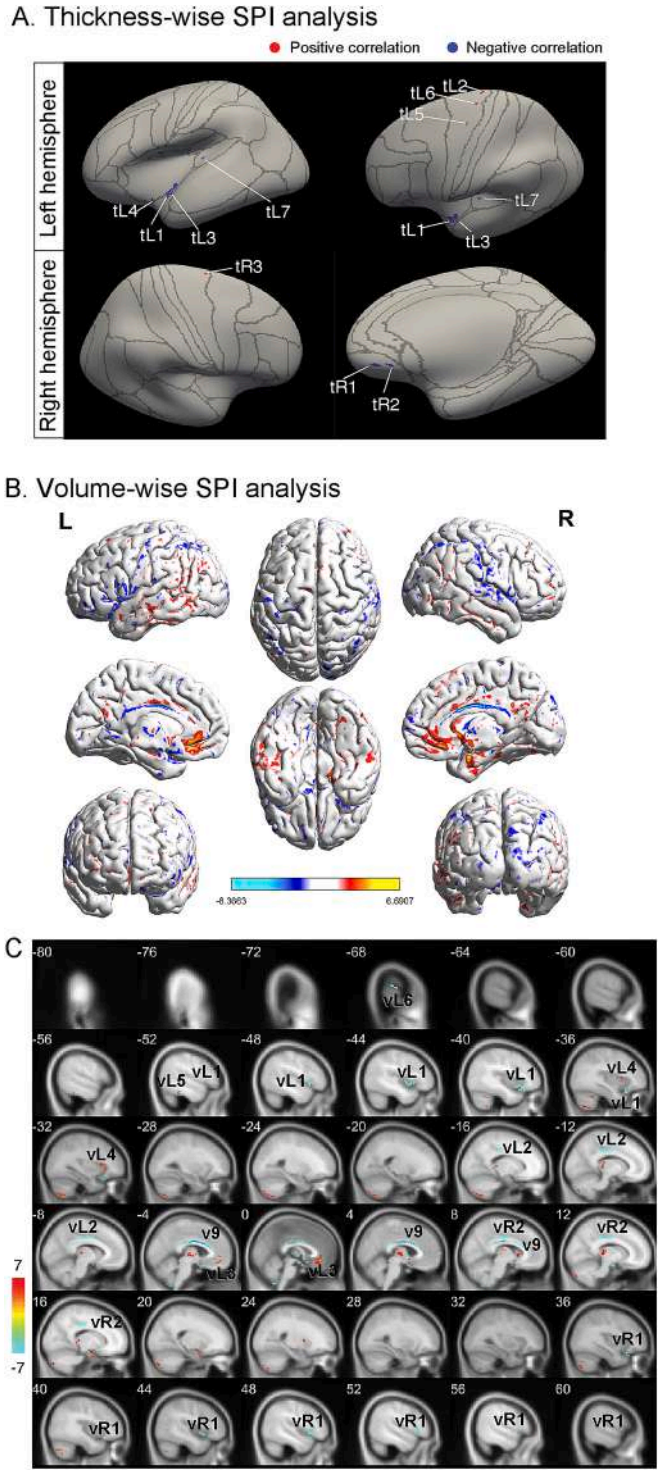


*(caption on next column)*

**Fig. 2.** High SPI clusters were restricted in certain Brodmann areas.
(**A**) The inflated fsaverage space showing clusters of connected vertexes with significantly changed SPI in schizophrenia patients compared to healthy controls (FWE-corrected $p < 0.05$). The grey lines represent the boundaries of the Brodmann area. Red denotes clusters where SZ is significantly larger than HC, while blue indicates brain regions where HC is significantly larger than SZ. (**B**) The render view of the left medial side of the left hemisphere and right medial side of the right hemisphere showing clusters of connected voxels with significantly changed SPI in schizophrenia patients compared to healthy controls (FEW-corrected $p < 0.001$, cluster size >100 voxels) using BrainNet Viewer (https://www.nitrc.org/projects/bnv/). **(C)** Sagittal sections showing clusters of connected voxels with significantly changed SPI in schizophrenia patients compared to healthy controls (FEW-corrected p < 0.001, cluster size >100 voxels) using xjView toolbox (http://www.alivelearn.net/xjview). Slice position was indicated by numbers from the left hemisphere (negative number) to the right hemisphere (positive number). (For interpretation of the references to color in this figure legend, the reader is referred to the web version of this article.)

identified affected BA (Supplementary Fig. 3B and Supplementary Table 3), we selected individuals with SZ with significant differences in the identified areas using a one-sample *t*-test versus all HC samples. The GWAS was then performed using the extracted SZ samples and all HC samples to identify associated SNPs in thickness-wise and volume-wise SPI analyses (Supplementary Fig. 3C). In GWAS results of thickness-wise SPI analysis, SNPs on chromosomes 10 (rs670625) and 15 (rs12232282) exhibited highly similar patterns across affected BAs. Although significant SNP levels were generally lower for volume-wise SPI analysis, SNPs on chromosomes 10 (rs670625) and 15 (rs12232282) were also identified in most of the affected BAs. This highly identical pattern across affected BAs in both thickness-wise and volume-wise analysis indicated a consistent disease-associated relationship between certain SNPs and local structural alterations in the SZ group versus the HC group (Fig. 3C). In addition, the identified SNPs and their correlations showed some variability across affected BAs, reflecting dynamic levels of genetic factors on different functional areas of the cerebral cortex, as observed in morphological measurements. To assess the presence of abnormal genetic variants in individuals with SZ, we compared genotype distribution between SZ and HCs (Fig. 3D). The majority of genotypes in the HC group were significantly decreased in the SZ group, with an increase in heterozygous genotypes. Some SNPs showed a higher proportion of individuals with SZ having the homozygous genotype with the minor allele than HCs (Fig. 3D). In support of this notion, the odds ratio, minor allele frequency, and *p*-value of association tests all suggested the apparent changes in SNPs in individuals with SZ (Supplementary Table 4).

Finally, the identified SNPs were mapped to the genes using positional and expression quantitative trait loci (eQTL) on the FUMA GWAS server. Three genes (CHRNA5, MORF4L1, TMED3) from rs12232282 corresponded to half of the identified BAs. Two genes (FAM160A1, GATB) from rs79082682 and two genes (NRBF2, REEP3) from rs1255496 corresponded to certain BAs. The variable association between SNPs/mapped genes and affected BAs suggested diverse effects of genetic variants on local structural changes in the cerebral cortex, spanning a wide range of functional areas or limited to specific regions (Supplementary Table 5).

### 3.3. Associations of SNPs with changes in BAs

In the GWAS analysis, we found conserved genetic variants were identified from different affected BAs (Fig. 3C). We then asked whether this conservation arises from the high similarity among individual lists, where individuals with SZ exhibit significant differences in the identified BAs compared to HC, or if it results from varying impacts of specific genetic variants on different BAs. To address this, we assessed the similarity of individual lists across affected BAs using the Jaccard index,

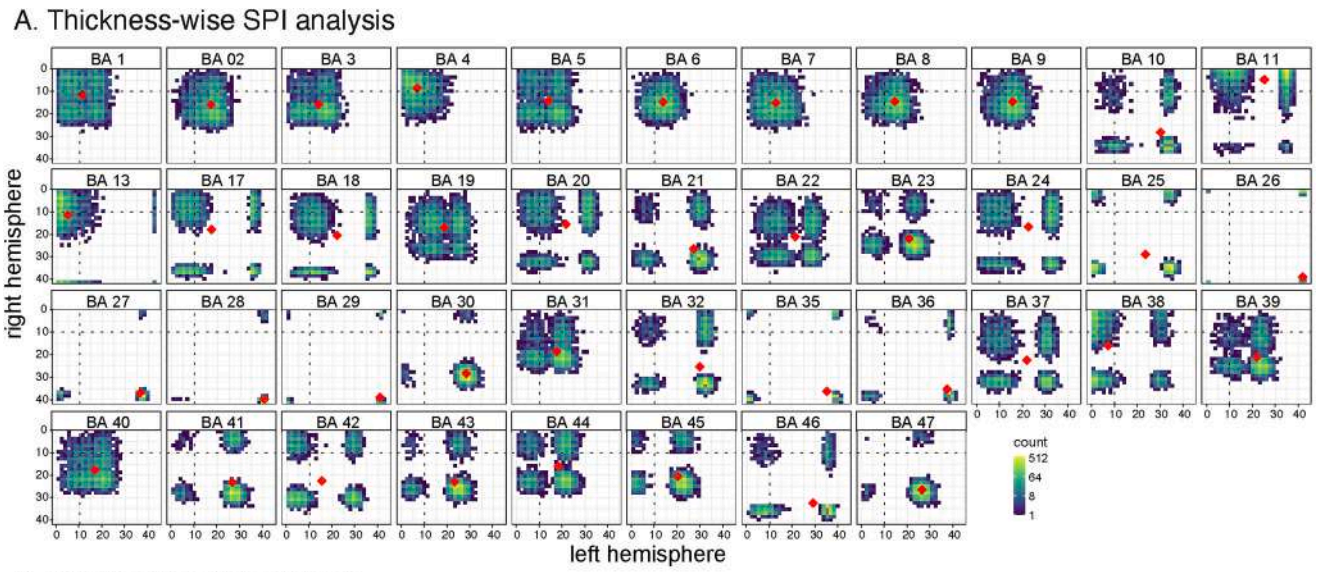


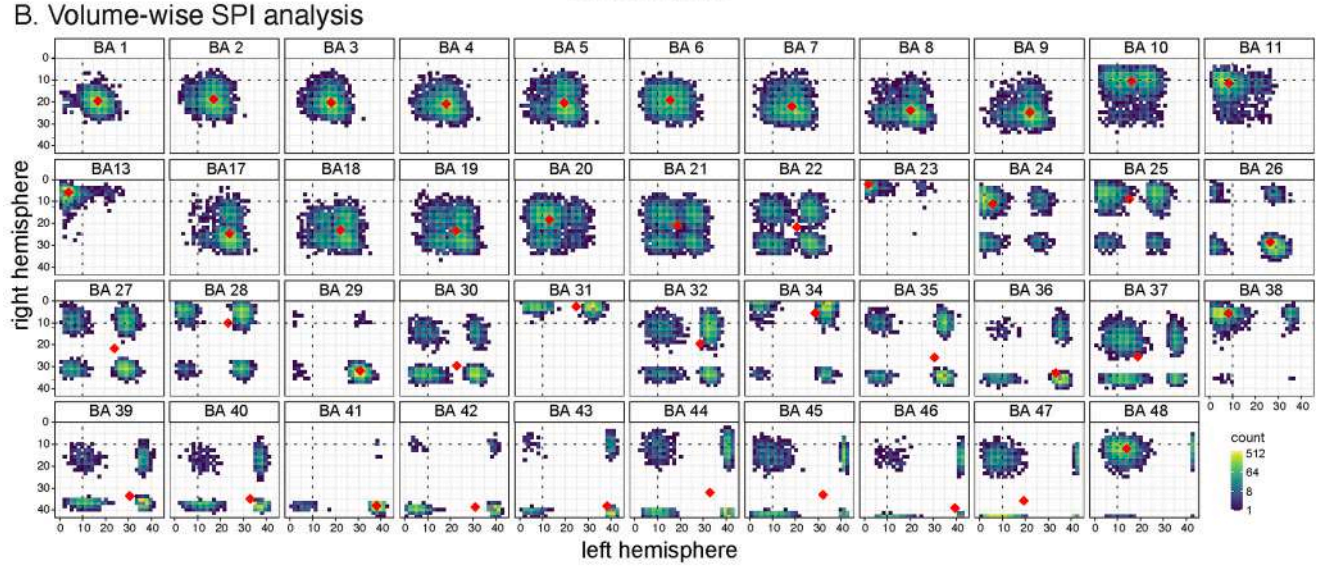


C

| SPI-hemi | area | SNPs | | | |
|---|---|---|---|---|---|
| thickness_lh | BA 4 | rs12232282 | | | |
| thickness_lh | BA 13 | rs670625 | rs12232282 | | |
| thickness_lh | BA 38 | rs670625 | rs12232282 | | |
| thickness_lh | BA 42 | rs670625 | rs12232282 | | |
| thickness_rh | BA 4 | rs75178723 | rs12232282 | | |
| thickness_rh | BA 11 | rs79082682 | rs1255496 | rs670625 | rs12232282 |
| volume_lh | BA 11 | NA | | | |
| volume_lh | BA 13 | rs12232282 | | | |
| volume_lh | BA 23 | rs670625 | | | |
| volume_lh | BA 24 | rs12232282 | | | |
| volume_lh | BA 37 | NA | | | |
| volume_lh | BA 38 | rs670625 | rs12232282 | | |
| volume_lh | BA 42 | NA | | | |
| volume_rh | BA 13 | rs670625 | | | |
| volume_rh | BA 23 | rs670625 | | | |
| volume_rh | BA 25 | NA | | | |
| volume_rh | BA 31 | rs670625 | rs12232282 | | |
| volume_rh | BA 34 | NA | | | |
| volume_rh | BA 38 | NA | | | |
| volume_rh | BA 47 | NA | | | |

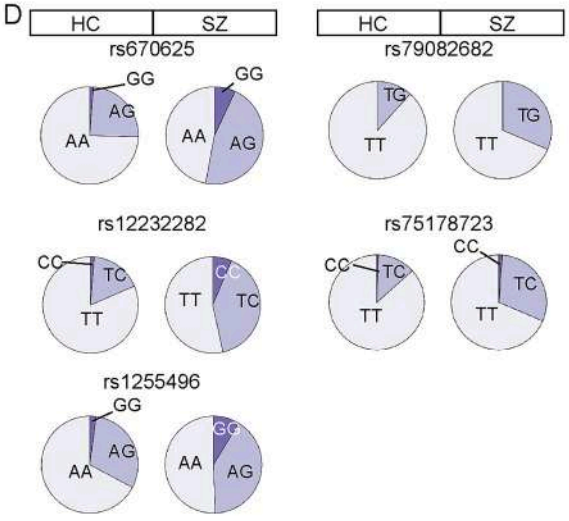


**Fig. 3.** Genetic variants are correlated to the distinct BAs in SZ group.
(**A-B**) The density plots show the results of the permutation test ($n = 500$) of the affected vertices/voxels ratio analysis in thickness-wise SPI analysis (**A**) and volume-wise SPI analysis (**B**). (**C**) The table shows the associated SNPs in the affected BAs. rh, right hemisphere. lh, left hemisphere. (**D**) Pie charts showing the distribution of SNP genotypes (rs75178723, rs12232282, rs670625, rs79082682, and rs1255496) in HC group and SZ group.

which calculates the proportion of intersecting populations in the union of populations between two BAs.

The overall mean similarity across 19 identified BAs was 33.95 %. The mean similarity within areas for thickness-wise SPI analysis, volume-wise SPI analysis, and thickness-wise versus volume-wise SPI analysis were 54.27 %, 34.67 %, and 29.33 %, respectively (Supplementary Fig. 4). The similarity of individual lists within thickness-wise SPI analysis (71.7 % to 42.96 %) was higher than that within volume-wise SPI analysis (59.38 % to 17.45 %). Comparison of affected BAs in the two SPI analyses showed the lowest mean similarity (47.83 % to 13.04 %). These results showed that the individual lists in the two SPI analyses were from different populations, which indicated that, unlike the highly conserved identified SNPs among the affected BAs, the ratio of overlapped individual lists was less than half the population. Nonetheless, we found higher similarity of the individual lists from the same BA in two hemispheres, such as the right BA4 and the left BA4 in thickness-wise SPI analysis (71.7 %), and the right BA38 and left BA38 in volume-wise SPI analysis (56.69 %), the known circuit-connected BAs, such as left BA13 and left BA38 (Nomi et al., 2018) in thickness-wise SPI analysis (63.87 %), and adjacent BAs, such as posterior cingulate cortex BA23 and BA31 in volume-wise SPI analysis (59.38 %) (Supplementary Fig. 4). Interestingly, a certain degree of overlapped individual lists may not result in the same SNP. For example, in volume-wise SPI analysis, rs670625 and rs12232282 were identified from the left BA38, but no SNP could be found in the right BA38, even though 56.69 % overlapped individual lists. This suggested that the high similarity of individual lists is not the cause of conserved genetic variants. And a single genetic variant may be associated with variable impacts.

### 3.4. Areal preference of the identified genes during human and mouse neocortical development

As SZ is suggested to be a neurodevelopmental disorder (Lewis and Levitt, 2002), at least partly by genetic factors, we thus investigated the dynamic expression pattern of SNP-mapped genes (Supplementary Table 4) in the developing cerebral cortex. We first analyzed the spatial expression pattern using single-cell transcriptomic analysis of the GW20 human developing neocortical dataset (Fig. 4A and Supplementary Fig. 4B) (Bhaduri et al., 2021). The results revealed candidate genes' areal preferential expression profiles in developing human neocortical cells (Fig. 4A-B). *CHRNA5* was enriched in neurons from the motor area, *MORF4L1, TMED3, and NRBF2* were enriched in neurons from the somatosensory area and progenitors, *REEP3* was enriched in progenitors, and *GATB* was enriched in neurons from both motor and somatosensory areas (Fig. 4A-B).

If these genes were involved in establishing BAs during the neocortical development, the dynamic expression pattern might be observed in the conserved areas in the developing mouse neocortex. To this, we investigate the temporal and spatial expression profiles of the identified genes in the developing mouse neocortex at E14.5, E18.5, and P4 using in situ hybridization analysis (Fig. 4C-D). The human and mouse data showed similar features, while temporal dynamics can be detected. For instance, *Morf411* in the mediolateral region, the future somatosensory area of the mouse neocortex, was barely detected at E14.5 but highly enriched at E18.5 and P4 (Fig. 4C-D). Interestingly, genes mapped from the same SNP may show opposite expression patterns, such as rs12232282-mapped genes Chrna5 and Morf4l1 in E14.5 and P4 brains. In both human and mouse data, *Chrna5* was enriched in the motor area, while *Morf411* was enriched in the non-motor areas. In addition to that, *Chrna5* was enriched in the future cingulate cortex in E18.5 brains, in contrast to *Morf4l1* and *Tmed3*, while their expression was generally low in the cingulate cortex of P4 brains (Fig. 4C-D).

### 3.5. Disrupting Morf4l1, Reep3 and Tmed3 expression impairs cortical cell fate

Next, we asked whether the identified genes were critical to establishing the functional maps during cortical development. Given that the cell composition and cytoarchitecture define the functions of the areas (Brodmann, 1909), we asked whether manipulating the identified gene expression would affect the cortical cell fate. To this, we utilized the CRISPR/Cas9 system with gRNAs to disrupt the start codon of the *Morf4l1, Reep3, or Tmed3* gene in the sensory cortex, consisting of a complete six-layer structure within the cerebral cortex (Brodmann, 1909). The CRISPR/Cas9 system was introduced to cortical progenitors through in-utero electroporation at E13.5, when the cortical progenitors are expected to produce both deep-layer cells (layer 5) and upper-layer cells (layer 4) in the cortex. We collected samples at P7 when functional circuits were established (Fig. 5A). Immunostaining results revealed that in the somatosensory area of control cortices, GFP-labeled cells were primarily positioned in layers 4 and 5, expressing layer 4 gene Rorβ and layer 5b gene Ctip2 (Fig. 5B-D). The distribution of GFP+ cells shifted downward in *Morf4l1* knockout cortices and upward in Reep3 or Tmed3 knockout cortices (Fig. 5B-C). Accompanied with the altered cell positioning, gene expression profiles of GFP+ cells were changed. Callosal projection neuron gene Brn2 was increased in the GFP+ cell population in *Morf4l1* knockout cortices, and layer 4 gene Rorβ was increased in the GFP+ cell population in *Reep3 and Tmed3* knockout cortices (Fig. 5B and D). These findings suggested that the presence of *Morf4l1, Reep3,* and *Tmed3* is critical to ensure the proper cell composition in establishing accurate functional maps.

## 4. Discussion

The integration of neuroimaging and DNA phenotypic data in this study provides insights into the connection between brain structures and genetic characteristics, allowing for the identification of specific brain regions associated with distinct phenotypes. Utilizing Brodmann's map for functional arealization facilitates the analysis of structural alterations within the cerebral cortex, linking them to cytoarchitecture and functional circuits. The key findings of this study were listed as follows. Firstly, the SPI demonstrated the changed local structural patterns, and the mapped BAs were identified in the individuals of SZ compared to the controls in cortical thickness and grey matter volume analysis. Secondly, the genetic variants and the mapped genes corresponding to the changed SPI in BAs were identified. Thirdly, the dynamic expression patterns of identified SNP-mapped genes showed the area preference in the single-cell RNA dataset of embryonic human cortical cells and in situ hybridization analysis of developing mouse neocortex. Lastly, the loss-of-function study revealed that the disruption of the SNP-mapped gene, *Morf4l1*, by the CRISPR/Cas9 system could affect cortical cell fate and position, suggesting the involvement of *Morf4l1* in establishing sensory cortex functionality. These findings deepen our understanding of the complex interplay between structural changes and their functional implications in individuals with SZ.

This study identified 15 BAs with enriched changed structural patterns in thickness and volume-wise SPI analysis (Supplementary Table 3). BA4, the primary motor area, is a crucial output gateway, delivering signals to neural tissue outside the neocortex. Layer 5 CTIP2-positive cells project efferent signals to the spinal cord, while layer 6 TBR1-positive cells project to the brainstem. Dysfunctions in affected BA4 may contribute to motor impairments seen in neurodegenerative diseases like Parkinson's disease (Lindenbach and Bishop, 2013) and mental disorders such as SZ (Abboud et al., 2017). BA11, located in the orbitofrontal cortex of the prefrontal cortex (PFC), plays a role in processing emotional and reward-related information (Rogers et al., 1999). Alterations in the orbitofrontal cortex, including BA11, have been linked to various mental disorders such as depression (Drevets, 2007), obsessive-compulsive disorder (Beucke et al., 2013), and SZ (Kanahara

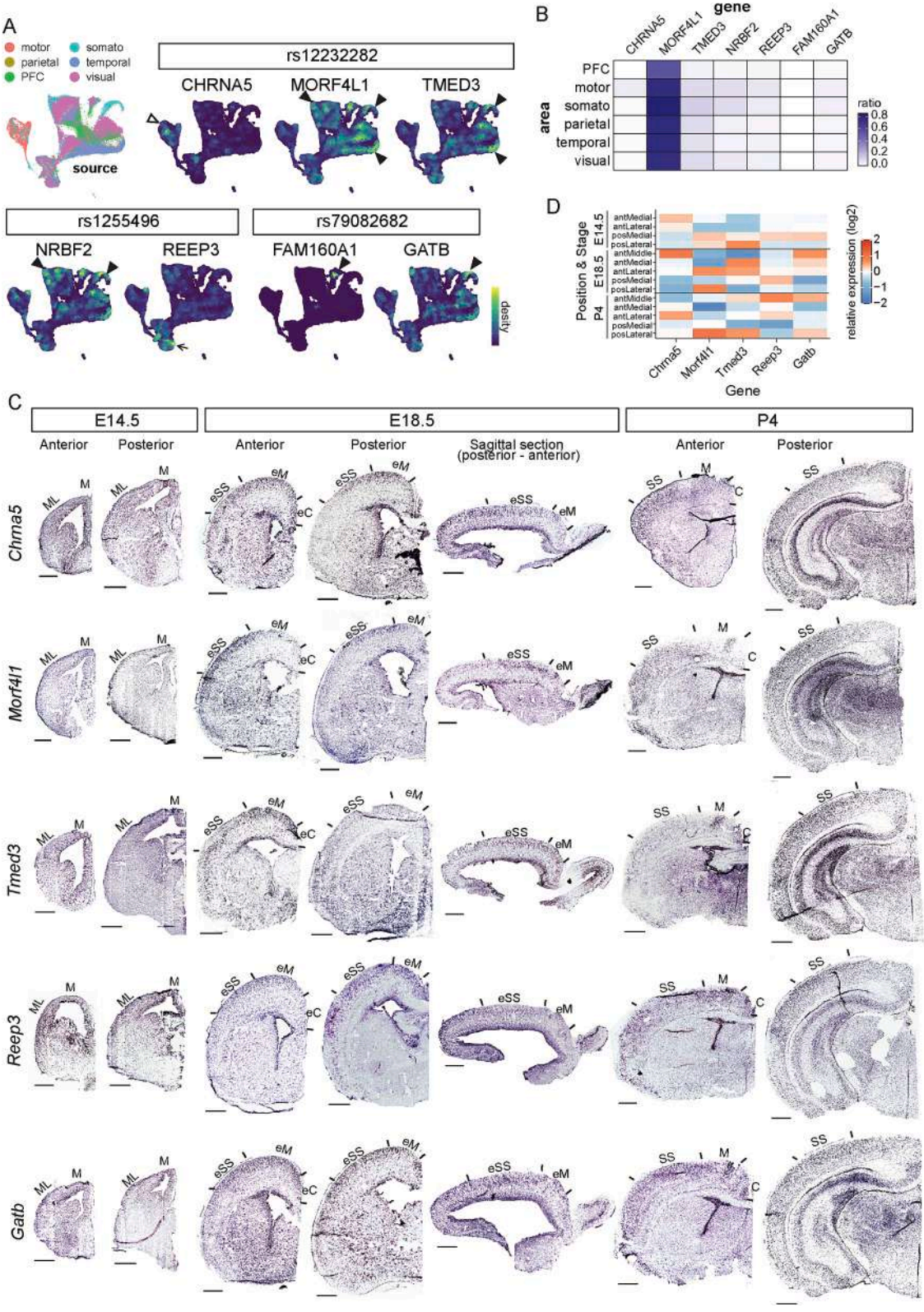


**Fig. 4.** Temporal and spatial expression pattern of candidate genes during cortical development.
(**A**) UMAP plots display the GW20 human neocortical cell dataset(Bhaduri et al., 2021), color-coded based on the origin and the gene expression levels correlated with the indicated SNP-mapped genes. Open arrowhead indicates high enrichment in the motor area, closed arrowheads indicate high enrichment in the non-motor areas, and arrow indicates high enrichment in progenitors. (**B**) The heatmap showing the ratio of gene-expressed cells in the source area. (**C**) ISH analysis of mRNA expression profiles of the indicated genes in the developing mouse neocortex at E14.5, E18.5, and P4 by in situ hybridization analysis. **(D)** Quantitative analysis of ISH signal intensity in 200um radial width of the indicated regions. Signals are relative to the mean of intensity in each time point. Scale bar = 500 μm. E, embryonic day; P, postnatal day; GW, gestational weeks; M, medial; ML, mediolateral; eSS, embryonic somatosensory area; eM, embryonic motor area; eC, embryonic cingulate area; SS, somatosensory area; M, motor area; C, cingulate area.

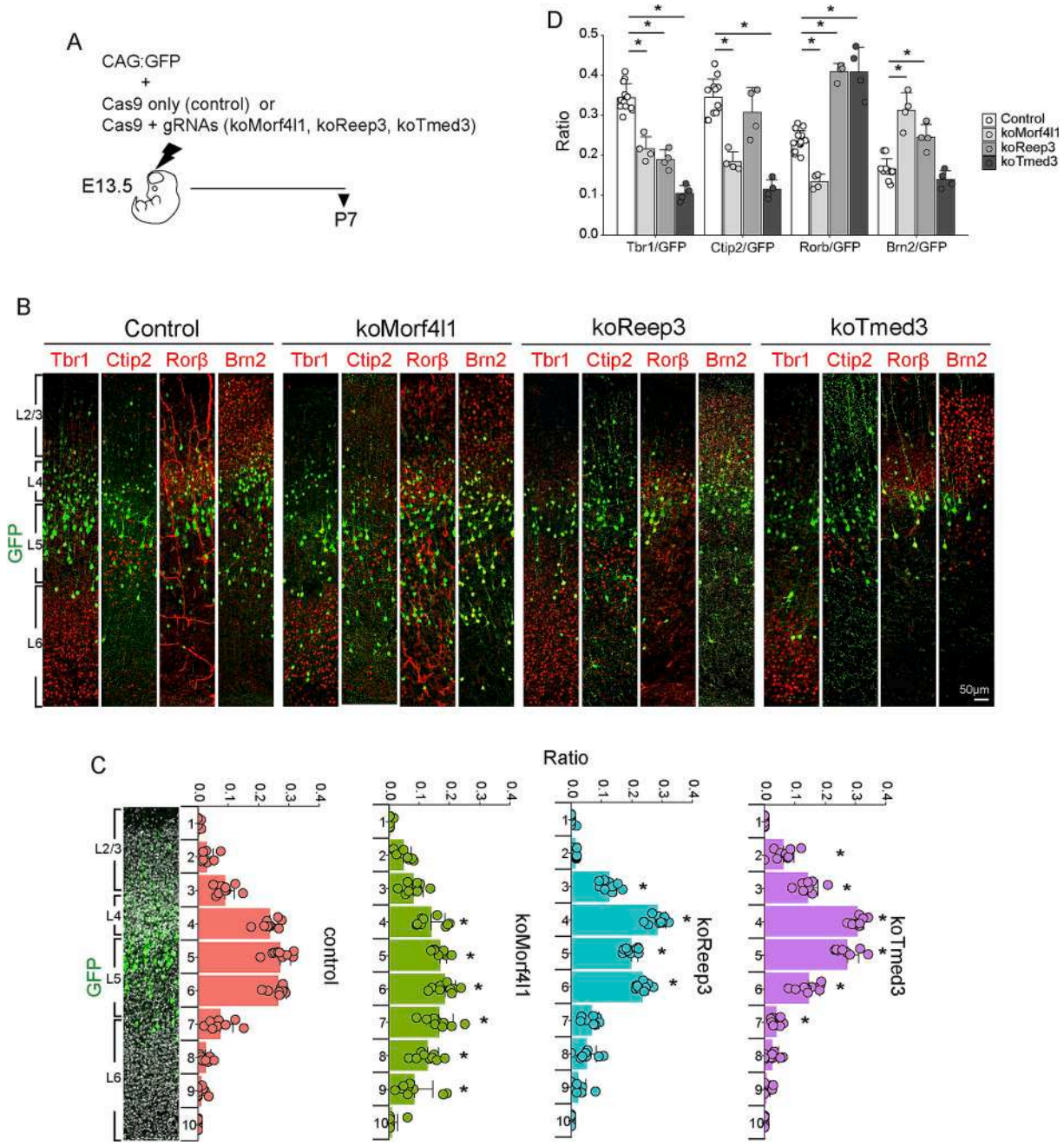


**Fig. 5.** Disrupting Morf4l1, Reep3 and Tmed3 expression affected cortical development.
(**A**) Schematic diagram of in-utero electroporation at E13.5 and sample collection at P7. Brains were electroporated with pCAG:GFP and Cas9 + gRNAs targeting the *Morf4l1, Reep3 or Tmed3* gene or Cas9 only as the control. (**B**) Immunostaining of P7 mouse cortices after in-utero electroporation at E13.5 using specific antibodies targeting GFP (green) and layer 6 gene Tbr1 (red), layer 5 gene Ctip2 (red), layer 4 gene Rorβ (red) and layer 2/3 and layer 5a gene Brn2 (grays), and Hoechst 33342 for nuclear counterstain (blue). Cortical layers were indicated. (**C**) Quantitative analysis of the distribution of GFP cells in the cortical plate. The cortical plate was divided into 10 BINs from the top layer 1 to the bottom of the cortical plate. (**D**) Quantitative analysis of the percentage of GFP-positive cells that express Tbr1, Ctip2, Rorβ, or Brn2. Biological repeats: control = 12, koMorf4l1 = 4, koReep3 = 4, and koTmed3 = 4. The scale bar represents mean ± SD. * represent *p*-value <0.05 compared to the control by student's *t*-test (excel software). (For interpretation of the references to color in this figure legend, the reader is referred to the web version of this article.)

et al., 2013). BA13, situated in the insula, serves as an integration hub connecting sensory areas (thalamus and sensory cortex) for multi-modal signal integration and the PFC (anterior cingulate, orbitofrontal, and medial PFC) for cognitive, emotional, and executive functions. Affected BA13 has been associated with neuropsychiatric disorders like anxiety, addiction, SZ, and autism (Gogolla, 2017). BAs 37, 38, and 42, located in different positions of the temporal lobe, showed decreased grey matter in individuals with SZ (Shenton et al., 1992). BA37 is involved in visual perception, word and object naming, recognition memory, and face recognition. Impaired BA37 could lead to word selection anomia observed in disorders like Alzheimer's disease (Thangavel et al., 2008) and negative symptoms in SZ (Potkin et al., 2002). BA42, part of the secondary auditory cortex and core Wernicke's area, is crucial for assigning meaning to words. Affected BA42 has been linked to hallucinations in SZ, with reduced thickness observed in individuals with SZ (Mørch-Johnsen et al., 2017). Moreover, our results revealed a

significantly positive association between the PANSS total score and cortical thickness in BA 29 (i.e., posterior cingulate cortex), as identified in the thickness-wise SPI map. A previous study found that grey matter volume alteration in the left isthmus of the cingulate cortex showed a positive correlation with both general psychopathology score and PANSS total score (Wei et al., 2021). Another study reported a trend suggesting a positive correlation between the connectivity of the posterior cingulate cortex and the anterior cingulate cortex with PANSS total score, particularly in patients with treatment-resistant schizophrenia (Wada et al., 2020). Our results, similar to previous studies, highlighted a consistent positive association between PANSS total scores and structural or functional changes in the posterior cingulate cortex, underscoring its potential role in the psychopathology of schizophrenia. However, no significant associations were identified between symptom severity and other brain regions in either the thickness-wise or volume-wise SPI maps in schizophrenia. We speculate that the individuals with schizophrenia in this study may be in a chronic phase with relatively stable symptom severity, which could account for the absence of significant associations between other symptom severity and other brain regions in both the thickness-wise and volume-wise SPIs.

Our genetic analysis grouped patients with significant SPI alterations within the identified BAs. Given the potential regulation of different brain regions and genetic variants by distinct mechanisms, it is plausible that patients are affected by diverse factors, potentially compensating for abnormal alterations in brain morphology and allele frequency. This approach, encompassing all patients in one analysis, may contribute to a more comprehensive understanding of the genetic landscape associated with SZ. The identified variants were mapped to 7 genes, with mRNA expression patterns observed in GW20 human cortical cells and 5 out of 7 genes observed in the mouse cerebral cortex at different developmental stages (E14.5, E18.5, and P4). Three of these genes, *MORF4L1*, *TMED3*, and *CHRNA5*, are correlated with a conserved significant SNP, rs12232282. *MORF4L1*, recognized as a critical factor associated with psychotic disorders, is part of the NuA4 histone acetyltransferase (HAT) complex, involved in histone acetylation and associated with various cellular processes. Knockdown of *MORF4L1* has demonstrated effects on cell proliferation, migration, and invasion, emphasizing its role in regulating gene expression (Sang et al., 2019). Additionally, *MORF4L1*, also known as *MRG15*, plays a crucial role in recognizing methylated histone protein (H3K36) and suppressing exon insertion into mRNA (Iwamori et al., 2016), impacting neural progenitor proliferation and cell fate determination (Chen et al., 2009). *TMED3*, a transmembrane protein, is implicated in Golgi organization and intracellular protein transport. Its increased expression in the prefrontal cortex during human development has been associated with color agnosia (Tanja et al., 2021). *CHRNA5*, part of the nicotinic acetylcholine receptor complex, has links to nicotine dependence, a risk factor for SZ (Ding and Hu, 2021). Studies have reported a genetic association between *CHRNA5* and SZ, particularly in the Han Chinese population (Zhan et al., 2019). While the basic functions of these identified genes are known, further research is essential to uncover their specific roles in the pathological mechanisms of SZ and the neural system during development.

Our findings highlight multiple functional areas specifically impacted in individuals with SZ, offering insights into potential genetic mechanisms influencing functional area establishment during cortical development. Furthermore, SPI analysis captured local structural variability within BAs and provided insights into both symmetric and asymmetric alterations in cortical regions associated with schizophrenia. We connected these structural patterns with specific genetic variants and SNP-mapped genes, highlighting how SPI can integrate structural and genetic data to elucidate potential neurodevelopmental mechanisms underlying these morphological changes. Moreover, SPI has the potential to complement traditional VBM by identifying regions with heightened variability or localized abnormalities, thereby enabling a more detailed and granular analysis of affected brain regions in future studies. However, several considerations should be taken into account. Firstly, the small sample size raises concerns about limited results surviving statistical thresholds and the potential influence of dataset features versus disease phenotypes. Although permutation random sampling and cluster correction were employed to mitigate false positives, replication with a larger independent dataset is crucial. Secondly, the impact of antipsychotic drugs on brain morphology in individuals with SZ should be considered in future studies to distinguish between pathological progression and drug effects. Lastly, accounting for covariates like onset age or illness duration would provide a more comprehensive understanding of SZ's pathological progression (DeLisi et al., 2006) and its impact on both structure and function.

## 5. Conclusion

Our study revealed region-specific morphological alterations, such as reduced cortical thickness and decreased grey matter volume in distinct functional areas, providing insights into the complex structural organization of the brain in SZ. We offered a more nuanced perspective on localized structural changes by utilizing the SPI at the vertex and voxel scales. The annotation of functional areas (i.e., BAs) further enables the classification of subsets of patients with SZ based on altered structural patterns. The low similarity among patient subsets across different regions highlighted the heterogeneity of traits within SZ. While this subdivision enhanced the precision of GWAS analysis, our study was limited by the relatively small sample size. Future research should address this limitation by incorporating larger datasets for validation, thereby increasing statistical power in regional analyses. This study outlines a pipeline for identifying local structural changes, their associated genetic causes, and potential molecular mechanisms underlying mental disorders. Additionally, these findings contribute to our understanding of the structural integrity of the cerebral cortex in supporting higher cognitive functions.

## Ethical statement

The study received approval from the Institutional Review Board of both Taipei Veterans General Hospital and National Yang Ming Chiao Tung University. All participants provided written informed consent.

## CRediT authorship contribution statement

**Pei-Shan Hou:** Writing – review & editing, Writing – original draft, Visualization, Validation, Supervision, Project administration, Methodology, Funding acquisition, Formal analysis, Data curation, Conceptualization. **Shu-Fei Lin:** Visualization, Validation, Formal analysis, Data curation. **Jun-Ding Zhu:** Visualization, Validation, Formal analysis, Data curation. **Chih-Yun Chung:** Methodology, Formal analysis, Data curation. **Shih-Jen Tsai:** Writing – review & editing, Supervision, Resources, Project administration, Methodology. **Albert C. Yang:** Writing – review & editing, Supervision, Resources, Project administration, Methodology, Funding acquisition, Conceptualization.

## Declaration of competing interest

The authors declare that they have no known competing financial interests or personal relationships that could have appeared to influence the work reported in this paper.

## Data availability

The data of this study are available from the corresponding author upon reasonable request.

## Acknowledgment

This work was supported by the National Science and Technology

Council (NSTC), Taiwan (Grant No. 111-2634-F-A49-014-, 112-2321-B-A49-013, and 112-2823-8-A49-001 for A.C.Y. and 108-2320-B-010 -046 -MY3 and 111-2314-B-A49 -053 -MY3 for P.H.), Taipei Veterans General Hospital, Taipei, Taiwan (Grant No. V112C-054 for A.C.Y.), YEN TJING LING MEDICAL FOUNDATION (Grant No. CI-110-4 for P.H.) and National Health Research Institutes grant (Grant No. NHRI-EX110-11007NC for P.H.). The Mt. Jade Young Scholarship Award from the Ministry of Education, Taiwan, also supported Dr. A.C.Y.. The Brain Research Center financially supported this work, National Yang Ming Chiao Tung University, from The Featured Areas Research Center Program within the framework of the Higher Education Sprout Project by the Ministry of Education (MOE) in Taiwan (Grant No. 112 W32101).

## Appendix A. Supplementary data

Supplementary data to this article can be found online at https://doi.org/10.1016/j.pnpbp.2025.111270.

## References


Abboud, R., Noronha, C., Diwadkar, V.A., 2017. Motor system dysfunction in the schizophrenia diathesis: neural systems to neurotransmitters. Eur. Psychiatry 44, 125–133. https://doi.org/10.1016/j.eurpsy.2017.04.004.

François Aguet, Shankara Anand, Kristin G Ardlie, Stacey Gabriel, Gad A Getz, A G., Kane Hadley, Robert E Handsaker, Katherine H Huang, Seva Kashin, Xiao Li, Daniel G MacArthur, Samuel R Meier, Jared L Nedzel, Duyen T Nguyen, Ayellet V Segrè, Ellen Todres, Brunilda Balliu, Alvaro N Barbeira, Alexis Battle, Rodrigo Bonazzola, Andrew Brown, C. D. B., Stephane E Castel, Donald F Conrad, Daniel J Cotter, Nancy Cox, Sayantan Das, Olivia M de Goede, Emmanouil T Dermitzakis, Jonah Einson, Barbara E Engelhardt, Eleazar Eskin, Tiffany Y Eulalio, Nicole M Ferraro, Elise D Flynn, Laure Fresard, E. R. G., Diego Garrido-Martín, Nicole R Gay, Michael J Gloudemans, Roderic Guigó, Andrew R Hame, Yuan He, Paul J Hoffman, Farhad Hormozdiari, Lei Hou, Hae Kyung Im, Brian Jo, Silva Kasela, Manolis Kellis, Sarah Kim-Hellmuth, Alan Kwong, Tuuli Lappalainen, X. L., Yanyu Liang, Serghei Mangul, Pejman Mohammadi, Stephen B Montgomery, Manuel Muñoz-Aguirre, Daniel C Nachun, Andrew B Nobel, Meritxell Oliva, YoSon Park, Yongjin Park, Princy Parsana, Abhiram S Rao, Ferran Reverter, John M Rouhana, Chiara Sabatti, A. S., Matthew Stephens, Barbara E Stranger, Benjamin J Strober, Nicole A Teran, Ana Viñuela, Gao Wang, Xiaoquan Wen, Fred Wright, Valentin Wucher, Yuxin Zou, Pedro G Ferreira, Gen Li, Marta Melé, Esti Yeger-Lotem, Mary E Barcus, Debra Bradbury, T. K., Jeffrey A McLean, Liqun Qi, Karna Robinson, Nancy V Roche, Anna M Smith, Leslie Sobin, David E Tabor, Anita Undale, Jason Bridge, Lori E Brigham, Barbara A Foster, Bryan M Gillard, Richard Hasz, Marcus Hunter, Christopher Johns, M. J., Ellen Karasik, Gene Kopen, William F Leinweber, Alisa McDonald, Michael T Moser, Kevin Myer, Kimberley D Ramsey, Brian Roe, Saboor Shad, Jeffrey A Thomas, Gary Walters, Michael Washington, Joseph Wheeler, Scott D Jewell, Daniel C Rohrer, D. R. V., David A Davis, Deborah C Mash, Philip A Branton, Laura K Barker, Heather M Gardiner, Maghboeba Mosavel, Laura A Siminoff, Paul Flicek, Maximilian Haeussler, Thomas Juettemann, W James Kent, Christopher M Lee, Conner C Powell, K. R. R. Magali Ruffier, Dan Sheppard, Kieron Taylor, Stephen J Trevanion, Daniel R Zerbino, Nathan S Abell, Joshua Akey, Lin Chen, Kathryn Demanelis, Jennifer A Doherty, Andrew P Feinberg, Kasper D Hansen, Peter F Hickey, Farzana Jasmine, L. J., Rajinder Kaul, Muhammad G Kibriya, Jin Billy Li, Qin Li, Shin Lin, Sandra E Linder, Brandon L Pierce, Lindsay F Rizzardi, Andrew D Skol, Kevin S Smith, Michael Snyder, John Stamatoyannopoulos, Hua Tang, Meng Wang, Latarsha J Carithers, P. G., Susan E Koester, A Roger Little, Helen M Moore, Concepcion R Nierras, Abhi K Rao, Jimmie B Vaught, Simona Volpi. (2020). The GTEx consortium atlas of genetic regulatory effects across human tissues. Science, 369(6509), 1318–1330. doi: https://doi.org/10.1126/science.aaz1776.

Banaj, N., Vecchio, D., Piras, F., De Rossi, P., Bustillo, J., Ciufolini, S., Dazzan, P., Di Forti, M., Dickie, E.W., Ford, J.M., Fuentes-Claramonte, P., Gruber, O., Guerrero-Pedraza, A., Hamilton, H.K., Howells, F.M., Kraemer, B., Lawrie, S.M., Mathalon, D. H., Murray, R.,…Piras, F., 2023. Cortical morphology in patients with the deficit and non-deficit syndrome of schizophrenia: a worldwide meta- and mega-analyses. Mol. Psychiatry. https://doi.org/10.1038/s41380-023-02221-w.

Beucke, J.C., Sepulcre, J., Talukdar, T., Linnman, C., Zschenderlein, K., Endrass, T., Kaufmann, C., Kathmann, N., 2013. Abnormally high degree connectivity of the orbitofrontal cortex in obsessive-compulsive disorder. JAMA Psychiatry 70 (6), 619–629. https://doi.org/10.1001/jamapsychiatry.2013.173.

Bhaduri, A., Sandoval-Espinosa, C., Otero-Garcia, M., Oh, I., Yin, R., Eze, U.C., Nowakowski, T.J., Kriegstein, A.R., 2021. An atlas of cortical arealization identifies dynamic molecular signatures. Nature 598 (7879), 200–204. https://doi.org/10.1038/s41586-021-03910-8.

Bora, E., Fornito, A., Radua, J., Walterfang, M., Seal, M., Wood, S.J., Yücel, M., Velakoulis, D., Pantelis, C., 2011. Neuroanatomical abnormalities in schizophrenia: A multimodal voxelwise meta-analysis and meta-regression analysis. Schizophr. Res. 127 (1), 46–57. https://doi.org/10.1016/j.schres.2010.12.020.

Brodmann, K., 1909. Vergleichende Lokalisationslehre der Großhirnrinde. Barth, Leipzig.

Care, I., O. L. A. R. C. O., & Animals, U. O. L, 1986. Guide for the care and use of laboratory animals. US Department of Health and Human Services, Public Health Service, National.

Chang, C.C., Chow, C.C., Tellier, L.C., Vattikuti, S., Purcell, S.M., Lee, J.J., 2015. Second-generation PLINK: rising to the challenge of larger and richer datasets. Gigascience 4, 7. https://doi.org/10.1186/s13742-015-0047-8.

Chen, M., Takano-Maruyama, M., Pereira-Smith, O.M., Gaufo, G.O., Tominaga, K., 2009. MRG15, a component of HAT and HDAC complexes, is essential for proliferation and differentiation of neural precursor cells. J. Neurosci. Res. 87 (7), 1522–1531. https://doi.org/10.1002/jnr.21976.

Dale, A.M., Fischl, B., Sereno, M.I., 1999. Cortical surface-based analysis: I. Segmentation and Surface Reconstruction. NeuroImage 9 (2), 179–194. https://doi.org/10.1006/nimg.1998.0395.

Das, S., Forer, L., Schonherr, S., Sidore, C., Locke, A.E., Kwong, A., Vrieze, S.I., Chew, E. Y., Levy, S., McGue, M., Schlessinger, D., Stambolian, D., Loh, P.R., Iacono, W.G., Swaroop, A., Scott, L.J., Cucca, F., Kronenberg, F., Boehnke, M.,…Fuchsberger, C., 2016. Next-generation genotype imputation service and methods. Nat. Genet. 48 (10), 1284–1287. https://doi.org/10.1038/ng.3656.

Davatzikos, C., 2004. Why voxel-based morphometric analysis should be used with great caution when characterizing group differences. NeuroImage 23, 17–20.

DeLisi, L.E., Szulc, K.U., Bertisch, H.C., Majcher, M., Brown, K., 2006. Understanding structural brain changes in schizophrenia. Dialogues Clin. Neurosci. 8 (1), 71–78. https://doi.org/10.31887/DCNS.2006.8.1/ldelisi.

Destrieux, C., Fischl, B., Dale, A., Halgren, E., 2010. Automatic parcellation of human cortical gyri and sulci using standard anatomical nomenclature. Neuroimage 53 (1), 1–15. https://doi.org/10.1016/j.neuroimage.2010.06.010.

Ding, J.B., Hu, K., 2021. Cigarette smoking and schizophrenia: etiology, clinical, pharmacological, and treatment implications. Schizophr. Res. Treat. 2021, 7698030. https://doi.org/10.1155/2021/7698030.

Drevets, W.C., 2007. Orbitofrontal cortex function and structure in depression. Ann. N. Y. Acad. Sci. 1121, 499–527. https://doi.org/10.1196/annals.1401.029.

Etkin, A., Egner, T., Kalisch, R., 2011. Emotional processing in anterior cingulate and medial prefrontal cortex. Trends Cogn. Sci. 15 (2), 85–93. https://doi.org/10.1016/j.tics.2010.11.004.

Eyler, L.T., Chen, C.-H., Panizzon, M.S., Fennema-Notestine, C., Neale, M.C., Jak, A.J., Jernigan, T.L., Fischl, B.R., Franz, C.E., Lyons, M.J., Grant, M.D., Prom-Wormley, E. C., Seidman, L.J., Tsuang, M.T., Fiecas, M., Dale, A.M., Kremen, W.S., 2012. A comparison of heritability maps of cortical surface area and thickness and the influence of adjustment for whole brain measures: A magnetic resonance imaging twin study. Twin Res. Hum. Genet. 15, 304–314.

Fischl, B., 2012. FreeSurfer. NeuroImage 62 (2), 774–781. https://doi.org/10.1016/j.neuroimage.2012.01.021.

Fischl, B., Sereno, M.I., Tootell, R.B., Dale, A.M., 1999. High-resolution intersubject averaging and a coordinate system for the cortical surface. Hum. Brain Mapp. 8 (4), 272–284. https://doi.org/10.1002/(sici)1097-0193(1999)8:4<272::aid-hbm10>3.0.co;2-4.

Genomes Project, C, Auton, A., Brooks, L.D., Durbin, R.M., Garrison, E.P., Kang, H.M., Korbel, J.O., Marchini, J.L., McCarthy, S., McVean, G.A., Abecasis, G.R., 2015. A global reference for human genetic variation. Nature 526 (7571), 68–74. https://doi.org/10.1038/nature15393.

Gogolla, N., 2017. The insular cortex. Curr. Biol. 27 (12), R580–R586. https://doi.org/10.1016/j.cub.2017.05.010.

Herlin, B., Navarro, V., Dupont, S., 2021. The temporal pole: from anatomy to function-A literature appraisal. J. Chem. Neuroanat. 113, 101925. https://doi.org/10.1016/j.jchemneu.2021.101925.

Hou, P.S., Kumamoto, T., Hanashima, C., 2017. A sensitive and versatile in situ hybridization protocol for gene expression analysis in developing Amniote brains. Methods Mol. Biol. 1650, 319–334. https://doi.org/10.1007/978-1-4939-7216-6_22.

Hou, P.S., Miyoshi, G., Hanashima, C., 2019. Sensory cortex wiring requires preselection of short- and long-range projection neurons through an Egr-Foxg1-COUP-TFI network. Nat. Commun. 10 (1), 3581. https://doi.org/10.1038/s41467-019-11043-w.

Iwamori, N., Tominaga, K., Sato, T., Riehle, K., Iwamori, T., Ohkawa, Y., Coarfa, C., Ono, E., Matzuk, M.M., 2016. MRG15 is required for pre-mRNA splicing and spermatogenesis. Proc. Natl. Acad. Sci. 113 (37), E5408–E5415. https://doi.org/10.1073/pnas.1611995113.

Kanahara, N., Sekine, Y., Haraguchi, T., Uchida, Y., Hashimoto, K., Shimizu, E., Iyo, M., 2013. Orbitofrontal cortex abnormality and deficit schizophrenia. Schizophr. Res. 143 (2–3), 246–252. https://doi.org/10.1016/j.schres.2012.11.015.

Kety, S.S., 1987. The significance of genetic factors in the etiology of schizophrenia: results from the national study of adoptees in Denmark. J. Psychiatr. Res. 21 (4), 423–429. https://doi.org/10.1016/0022-3956(87)90089-6.

LaPoint, M.R., Chhatwal, J.P., Sepulcre, J., Johnson, K.A., Sperling, R.A., Schultz, A.P., 2017. The association between tau PET and retrospective cortical thinning in clinically normal elderly. Neuroimage 157, 612–622. https://doi.org/10.1016/j.neuroimage.2017.05.049.

Lewis, D.A., González-Burgos, G., 2008. Neuroplasticity of neocortical circuits in schizophrenia. Neuropsychopharmacology 33 (1), 141–165. https://doi.org/10.1038/sj.npp.1301563.

Lewis, D.A., Levitt, P., 2002. Schizophrenia as a disorder of neurodevelopment. Annu. Rev. Neurosci. 25, 409–432. https://doi.org/10.1146/annurev.neuro.25.112701.142754.

Lindenbach, D., Bishop, C., 2013. Critical involvement of the motor cortex in the pathophysiology and treatment of Parkinson's disease. Neurosci. Biobehav. Rev. 37 (10 Pt 2), 2737–2750. https://doi.org/10.1016/j.neubiorev.2013.09.008.

Loh, P.R., Danecek, P., Palamara, P.F., Fuchsberger, C., Y, A.R., H, K.F., Schoenherr, S., Forer, L., McCarthy, S., Abecasis, G.R., Durbin, R., A, L.P., 2016a. Reference-based phasing using the haplotype reference consortium panel. Nat. Genet. 48 (11), 1443–1448. https://doi.org/10.1038/ng.3679.

Loh, P.R., Palamara, P.F., Price, A.L., 2016b. Fast and accurate long-range phasing in a UK biobank cohort. Nat. Genet. 48 (7), 811–816. https://doi.org/10.1038/ng.3571.

Mørch-Johnsen, L., Nesvåg, R., Jørgensen, K.N., Lange, E.H., Hartberg, C.B., Haukvik, U. K., Kompus, K., Westerhausen, R., Osnes, K., Andreassen, O.A., Melle, I., Hugdahl, K., Agartz, I., 2017. Auditory cortex characteristics in schizophrenia: associations with auditory hallucinations. Schizophr. Bull. 43 (1), 75–83. https://doi.org/10.1093/schbul/sbw130.

Nomi, J.S., Schettini, E., Broce, I., Dick, A.S., Uddin, L.Q., 2018. Structural connections of functionally defined human insular subdivisions. Cereb. Cortex 28 (10), 3445–3456. https://doi.org/10.1093/cercor/bhx211.

Ozkan, A., MacDonald, J.L., Fame, R.M., Itoh, Y., Peter, M., Durak, O., Macklis, J.D., 2020. Specification of cortical projection neurons: Transcriptional mechanisms. In: Patterning and Cell Type Specification in the Developing CNS and PNS. Elsevier, pp. 427–459. https://doi.org/10.1016/B978-0-12-814405-3.00019-9.

Potkin, S.G., Alva, G., Fleming, K., Anand, R., Keator, D., Carreon, D., Doo, M., Jin, Y., Wu, J.C., Fallon, J.H., 2002. A PET study of the pathophysiology of negative symptoms in schizophrenia. Positron emission tomography. Am. J. Psychiatry 159 (2), 227–237. https://doi.org/10.1176/appi.ajp.159.2.227.

Purcell, S., Neale, B., Todd-Brown, K., Thomas, L., Ferreira, M.A., Bender, D., Maller, J., Sklar, P., de Bakker, P.I., Daly, M.J., Sham, P.C., 2007. PLINK: a tool set for whole-genome association and population-based linkage analyses. Am. J. Hum. Genet. 81 (3), 559–575. https://doi.org/10.1086/519795.

Ramasamy, A., Trabzuni, D., Guelfi, S., Varghese, V., Smith, C., Walker, R., De, T., Coin, L., de Silva, R., Cookson, M.R., Singleton, A.B., Hardy, J., Ryten, M., Weale, M. E., 2014. Genetic variability in the regulation of gene expression in ten regions of the human brain. Nat. Neurosci. 17 (10), 1418–1428. https://doi.org/10.1038/nn.3801.

Rimol, L.M., Rimol, L.M., Panizzon, M.S., Fennema-Notestine, C., Eyler, L.T., Fischl, B.R., Franz, C.E., Hagler, D.J., Lyons, M.J., Neale, M.C., Pacheco, J.L., Perry, M., Schmitt, J.E., Grant, M.D., Seidman, L.J., Thermenos, H.W., Tsuang, M.T., Eisen, S. A., Kremen, W.S., Dale, A.M., 2010. Cortical thickness is influenced by regionally specific genetic factors. Biol. Psychiatry 67, 493–499.

Rogers, R.D., Owen, A.M., Middleton, H.C., Williams, E.J., Pickard, J.D., Sahakian, B.J., Robbins, T.W., 1999. Choosing between small, likely rewards and large, unlikely rewards activates inferior and orbital prefrontal cortex. J. Neurosci. 19 (20), 9029–9038. https://doi.org/10.1523/JNEUROSCI.19-20-09029.1999.

Rolls, E.T., Huang, C.C., Lin, C.P., Feng, J., Joliot, M., 2020. Automated anatomical labelling atlas 3. Neuroimage 206, 116189. https://doi.org/10.1016/j.neuroimage.2019.116189.

Rubinacci, S., Delaneau, O., Marchini, J., 2020. Genotype imputation using the positional burrows wheeler transform. PLoS Genet. 16 (11), e1009049. https://doi.org/10.1371/journal.pgen.1009049.

Sakuma, T., Nishikawa, A., Kume, S., Chayama, K., Yamamoto, T., 2014. Multiplex genome engineering in human cells using all-in-one CRISPR/Cas9 vector system. Sci. Rep. 4, 5400. https://doi.org/10.1038/srep05400.

Sang, Y., Zhang, R., Sun, L., Chen, K.K., Li, S.W., Xiong, L., Peng, Y., Zeng, L., Huang, G., 2019. MORF4L1 suppresses cell proliferation, migration and invasion by increasing p21 and E-cadherin expression in nasopharyngeal carcinoma. Oncol. Lett. 17 (1), 294–302. https://doi.org/10.3892/ol.2018.9588.

Schlaepfer, T.E., Harris, G.J., Tien, A.Y., Peng, L.W., Lee, S., Federman, E.B., Chase, G.A., Barta, P.E., Pearlson, G.D., 1994. Decreased regional cortical gray matter volume in schizophrenia. Am. J. Psychiatry 151 (6), 842–848. https://doi.org/10.1176/ajp.151.6.842.

Sheffield, J.M., Rogers, B.P., Blackford, J.U., Heckers, S., Woodward, N.D., 2020. Insula functional connectivity in schizophrenia. Schizophr. Res. 220, 69–77. https://doi.org/10.1016/j.schres.2020.03.068.

Shenton, M.E., Kikinis, R., Jolesz, F.A., Pollak, S.D., LeMay, M., Wible, C.G., Hokama, H., Martin, J., Metcalf, D., Coleman, M., et al., 1992. Abnormalities of the left temporal lobe and thought disorder in schizophrenia. A quantitative magnetic resonance imaging study. N. Engl. J. Med. 327 (9), 604–612. https://doi.org/10.1056/nejm199208273270905.

Shepherd, A.M., Matheson, S.L., Laurens, K.R., Carr, V.J., Green, M.J., 2012. Systematic meta-analysis of insula volume in schizophrenia. Biol. Psychiatry 72 (9), 775–784. https://doi.org/10.1016/j.biopsych.2012.04.020.

Sugihara, G., Oishi, N., Son, S., Kubota, M., Takahashi, H., Murai, T., 2017. Distinct patterns of cerebral cortical thinning in schizophrenia: A neuroimaging data-driven approach. Schizophr. Bull. 43 (4), 900–906. https://doi.org/10.1093/schbul/sbw176.

Sullivan, P.F., Kendler, K.S., Neale, M.C., 2003. Schizophrenia as a complex trait: evidence from a Meta-analysis of twin studies. Arch. Gen. Psychiatry 60 (12), 1187–1192. https://doi.org/10.1001/archpsyc.60.12.1187.

Tanja, C., Nijboer, E.V.S.H., van Haaften, Gijs W., van Zandvoort, Martine J., van der Spek, Peter J., Troelstra, Christine, de Kovel, Carolien, Koeleman, Bobby P.C., van der Zwaag, Bert, Brilstra, Eva H., Burbach, J. Peter H., 2021. Identification of candidate genes for developmental colour agnosia in a single unique family.

Thangavel, R., Sahu, S.K., Van Hoesen, G.W., Zaheer, A., 2008. Modular and laminar pathology of Brodmann's area 37 in Alzheimer's disease. Neuroscience 152 (1), 50–55. https://doi.org/10.1016/j.neuroscience.2007.12.025.

van Erp, T.G.M., Walton, E., Hibar, D.P., Schmaal, L., Jiang, W., Glahn, D.C., Pearlson, G. D., Yao, N., Fukunaga, M., Hashimoto, R., Okada, N., Yamamori, H., Bustillo, J.R., Clark, V.P., Agartz, I., Mueller, B.A., Cahn, W., de Zwarte, S.M.C., Hulshoff Pol, H., E.,…Turner, J. A., 2018. Cortical brain abnormalities in 4474 individuals with schizophrenia and 5098 control subjects via the enhancing neuro imaging genetics through Meta analysis (ENIGMA) consortium. Biol. Psychiatry 84 (9), 644–654. https://doi.org/10.1016/j.biopsych.2018.04.023.

Wada, M., Nakajima, S., Tarumi, R., Masuda, F., Miyazaki, T., Tsugawa, S., Ogyu, K., Honda, S., Matsushita, K., Kikuchi, Y., Fujii, S., Blumberger, D.M., Daskalakis, Z.J., Mimura, M., Noda, Y., 2020. Resting-state isolated effective connectivity of the cingulate cortex as a neurophysiological biomarker in patients with severe treatment-resistant schizophrenia. J Pers Med 10 (3). https://doi.org/10.3390/jpm10030089.

Wagstyl, K., Ronan, L., Whitaker, K.J., Goodyer, I.M., Roberts, N., Crow, T.J., Fletcher, P. C., 2016. Multiple markers of cortical morphology reveal evidence of supragranular thinning in schizophrenia. Transl. Psychiatry 6 (4), e780. https://doi.org/10.1038/tp.2016.43.

Wang, K., Li, M., Hakonarson, H., 2010. ANNOVAR: functional annotation of genetic variants from high-throughput sequencing data. Nucleic Acids Res. 38 (16), e164. https://doi.org/10.1093/nar/gkq603.

Wei, G.X., Ge, L., Chen, L.Z., Cao, B., Zhang, X., 2021. Structural abnormalities of cingulate cortex in patients with first-episode drug-naïve schizophrenia comorbid with depressive symptoms. Hum. Brain Mapp. 42 (6), 1617–1625. https://doi.org/10.1002/hbm.25315.

Westra, H.J., Peters, M.J., Esko, T., Yaghootkar, H., Schurmann, C., Kettunen, J., Christiansen, M.W., Fairfax, B.P., Schramm, K., Powell, J.E., Zhernakova, A., Zhernakova, D.V., Veldink, J.H., Van den Berg, L.H., Karjalainen, J., Withoff, S., Uitterlinden, A.G., Hofman, A., Rivadeneira, F.,…Franke, L., 2013. Systematic identification of trans eQTLs as putative drivers of known disease associations. Nat. Genet. 45 (10), 1238–1243. https://doi.org/10.1038/ng.2756.

Wickham, H., 2016. ggplot2: Elegant Graphics for Data Analysis. Springer-Verlag, New York. https://ggplot2.tidyverse.org.

Xia, M., Wang, J., He, Y., 2013. BrainNet viewer: a network visualization tool for human brain connectomics. PLoS One 8 (7), e68910. https://doi.org/10.1371/journal.pone.0068910.

Yan, C.G., Wang, X.D., Zuo, X.N., Zang, Y.F., 2016. DPABI: Data Processing & Analysis for (resting-state) brain imaging. Neuroinformatics 14 (3), 339–351. https://doi.org/10.1007/s12021-016-9299-4.

Zhan, D., Yao, Q., Fu, S., Liu, X., Zhou, J., Chen, D., Yu, C., 2019. Impact of CHRNA5 polymorphisms on the risk of schizophrenia in the Chinese Han population. Mol. Genet. Genomic Med. 7 (9), e869. https://doi.org/10.1002/mgg3.869.

Zhernakova, D. V., Deelen, P., Vermaat, M., van Iterson, M., van Galen, M., Arindrarto, W., van t Hof, P., Mei, H., van Dijk, F., Westra, H. J., Bonder, M. J., van Rooij, J., Verkerk, M., Jhamai, P. M., Moed, M., Kielbasa, S. M., Bot, J., Nooren, I., Pool, R.,… Franke, L. (2017). Identification of context-dependent expression quantitative trait loci in whole blood. Nat. Genet., 49(1), 139–145. doi:https://doi.org/10.1038/ng.3737.

Zhu, J.D., Tsai, S.J., Lin, C.P., Lee, Y.J., Yang, A.C., 2023a. Predicting aging trajectories of decline in brain volume, cortical thickness and fractional anisotropy in schizophrenia. Schizophrenia (Heidelb) 9 (1), 1. https://doi.org/10.1038/s41537-022-00325-w.

Zhu, J.D., Wu, Y.F., Tsai, S.J., Lin, C.P., Yang, A.C., 2023b. Investigating brain aging trajectory deviations in different brain regions of individuals with schizophrenia using multimodal magnetic resonance imaging and brain-age prediction: a multicenter study. Transl. Psychiatry 13 (1), 82. https://doi.org/10.1038/s41398-023-02379-5.